Experimental Temperature and Specific Absorption Rate Mapping Using MRI in a Transmit-receive Head Coil at 3.0T

Sukhoon Oh and Christopher M. Collins
Radiology, College of Medicine, The Pennsylvania State University, Hershey, Pennsylvania, United States

Abstract—

Introduction: MRI-based temperature mapping techniques have been applied to detect the temperature changes (ΔT) for a variety of applications, including during the thermoablation of tumors [1], and in verifying minimal temperature increment induced by EEG electrodes and/or its wires during MRI [2]. Although numerical calculations have been used to predict SAR distributions and resulting temperature increase throughout a sample due to excitation with the RF coil [3], experimental measurements with MR thermometry are rarely used for this purpose [4]. In this study, experimentally-acquired temperature maps are used to calculate the SAR distribution from a head-sized transmit-receive birdcage coil in an agar gel phantom at 3.0 T.

Method: Figure 1(a) shows the experimental arrangement of phantoms used in this study. Four reference phantoms of vegetable oil were placed strategically to allow for measurement of temporally and spatially varying phase drift in the case of long duration (30 min$\sim$) RF heating. In this study, however, the reference data was not necessary since heating was accomplished in a short enough duration that phase drift was negligible. A rectangular-shaped conductive agar-gel phantom containing 10 g/L of NaCl, 1 g/L of $CuSO_4$, and 7 g/L of agar, ($w \times h \times d$ $8.5 \times 7 \times 15\,\mathrm{cm}^3$) was used to measure heating and SAR. One fiber optic thermal sensor (OpSens, Canada) was placed at the center of the phantom (where minimum SAR is expected) to assess when thermal conduction effects became significant. Another thermal sensor was placed at a location of expected high SAR to assess when the temperature increases became nonlinear, also indicating significant impact of thermal conduction. Before the experiment began, the phantom was allowed to equilibrate with its surroundings within the magnet for several hours. A baseline phase image was acquired using a general gradient-echo (GRE) sequence (TR 70 ms, TE 20 ms, FOV $175 \times 175\,\mathrm{mm}^2$, matrix size 64×64, slice thickness 10 mm, NEX = 4, FA 30°, scan time about 18 seconds). Then, RF heating pulses were applied to the phantom for 2 minutes. A single quadrature birdcage coil was used for both heating and imaging purposes, in contrast to studies in diathermy and ablation using separate coils at different frequencies [5]. After the RF heating, another phase image was acquired as quickly as possible using the same parameters as the first GRE sequence except NEX = 1 (scan time about 4 seconds). During GRE acquisition, two axial slices were imaged at different locations (coil center, or $z = 0$, and 30 mm offset). The temperature change between the two GRE acquisition periods was assessed by the phase change, as according to the proton resonance frequency shift method of MR thermometry [6]. In a phantom, such as this, with no perfusion and no metabolic effects, and when heating rapidly from equilibrium before thermal conduction has a significant role, the Pennes bioheat equation [7] can be reduced to SAR = $c_{agar}\Delta T/dt$ where c_{agar} is the specific heat capacity of the agar-gel, ΔT is the temperature change, and dt is the duration of RF heating. The specific heat capacity of the agar-gel phantom was 4200 J/kg°C [8].

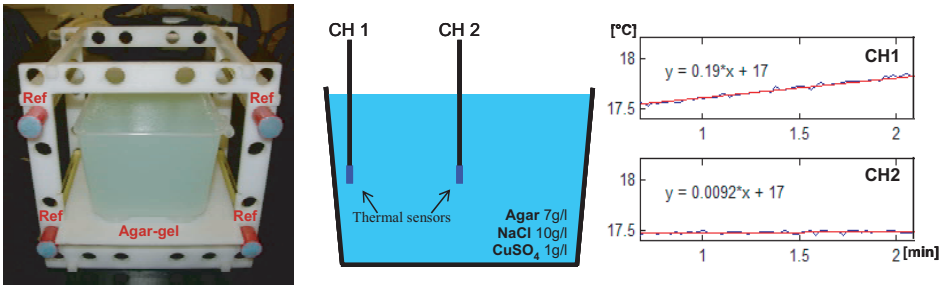

(a) (b) (c)

Figure 1: (a) Conductive agar-gel phantom ($w \times h \times d$ $8.5 \times 7 \times 15\mathrm{cm}^3$) and oil reference phantoms. (b) Setting of optic-fiber thermal sensors. (c) Temperature measurements and linear fitting for fiber optic data. Blue line indicates measurements and red line indicates linear fit.

Results and Discussion: Minimal temperature changes at the center of the phantom (channel 2) were seen at up to 3 minutes of heating, whereas a significant linear increase in temperature was seen near the edge of the phantom (channel 1) over the same time period (Figure 1(c)). The norm of residuals was compared between linear and cubic spline fits for the first 2 minutes of data. The norm of residuals of linear fitting was 0.177 whereas cubic spline was 0.175, indicating that the temperature was changing linearly for at least 2 minutes. In Figure 2(a), ΔT maps and SAR maps are shown on the axial slice passing through the center of the coil and phantom ($z = 0\,\text{mm}$). This result agrees well with expectations from electromagnetic theory, which predict that in the absence of wavelength effects, for a homogeneous B_1 field in an infinite phantom the SAR in the phantom should increase roughly with the square of the radial distance from the center. In Figure 2(b), the ΔT at the center is increased, due to an increased z value (30 mm), also an increase in the radial distance from the center leading to an expected increase in SAR. The maximum SAR near the edge of the phantom is greater at $z = 0$ partly due to the boundary conditions confining currents from other planes to this region on the center plane. The maximum SAR in one image voxel ($2.73 \times 2.73 \times 10\,\text{mm}^3$, or $0.074\,\text{cm}^3$) was found to be around 18 W/kg in Figure 2(a). While this simple demonstration in a phantom with no perfusion appears effective, the addition of perfusion (as well a noise and artifact from motion, etc.) would be expected to significantly hamper efforts to perform a similar experiment successfully *in-vivo* without extraordinary SAR levels. Our future experiments will focus on high-power RF heating in phantoms with transmit-arrays for the purposes of validating predictions from sophisticated numerical calculations.

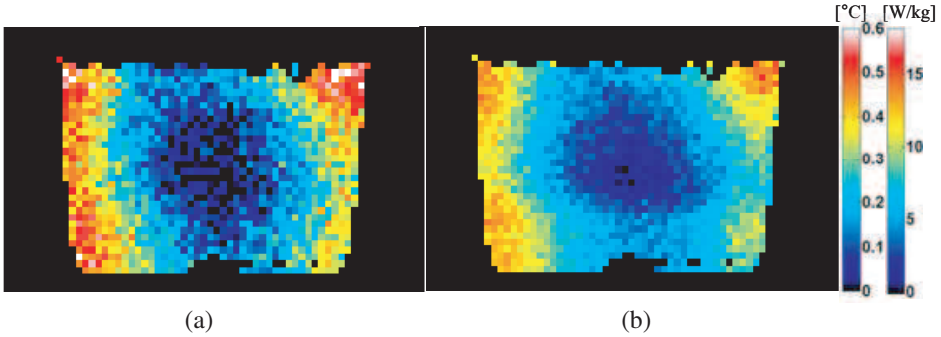

(a) (b)

Figure 2: Temperature change and SAR map at (a) $z = 0\,\text{mm}$ (coil center) and (b) $z = 30\,\text{mm}$. The scale bars on the right indicate temperature (°C) and SAR (W/kg), respectively.

ACKNOWLEDGMENT

Funding through NIH R01 EB000454.

REFERENCES

1. Steiner, et al., *Radiology*, Vol. 206, 803–810, 1998.
2. Angelone, et al., *Magn. Reson. Imag.*, Vol. 24, 801–812, 2006.
3. Collins, et al., *J. Magn. Reson. Imag.*, Vol. 19, 650–659, 2004.
4. Shapiro, et al., *Magn. Reson. In Med.*, Vol. 47, 492–498, 2002.
5. Behnia, et al., *Concepts Magn. Reson.*, Vol. 23B, No. 1, 1–15, 2004.
6. Ishihara, et al., *ISMRM*, 4803, Berlin, 1992.
7. Pennes, et al., *J. Appl. Physiol.*, Vol. 1, 93–122, 1948.
8. Armenean, et al., *Proceedings of the IEEE EMBS*, 501–504, Cancun, 2003.